Hybrid Nanogrid Systems for Future Small Communities

Farhad Shahnia

Abstract The power supply system of future communities can be considered in the form of a small microgrid or a nanogrid which is mainly based on renewable energy resources. Such a system can lead to a sustainable development of electrical systems and can help the current and future generations to access the benefits of electricity without adding more emissions and pollutions to the environment. A nanogrid should have adequate generation capacity in its distributed energy resources (DERs) to supply its demand in the off-grid status. It should also be able to exchange power with an existing utility feeder. The operation principle of a nanogrid is discussed in this chapter. A hybrid nanogrid may consist of one ac bus and one dc bus, which are connected via a power electronics-based converter. Some DERs and loads of the community will be connected to the ac bus of the nanogrid, while some DERs and loads will be connected to its dc bus. The converter facilitates power exchanges among the buses and also controls their voltages, during off-grid operation. The dynamic performance of a small community nanogrid is discussed in detail here.

Keywords Distributed energy resource · Nanogrid · Future communities

1 Introduction

Sustainable development is the core principle of maintaining our finite resources that are necessary for our future generations. Regarding electrical systems, sustainable development strongly depends on the application and control of renewable energy resources for electricity generation instead of the fossil fuels such as coal or gas. Also, it is highly desired to generate the electricity near the consumers such that minimum adverse impact is imposed on the nature when building long transmission and distribution lines. Environmental concerns, high electricity bills, and

F. Shahnia (✉)
School of Engineering and Information Technology, Murdoch University, Perth, Australia
e-mail: f.shahnia@murdoch.edu.au

B. Azzopardi (ed.), *Sustainable Development in Energy Systems*,
DOI 10.1007/978-3-319-54808-1_2

the financial incentives that are in place by the governments motivate the householders to install renewable energy-based distributed energy resources (DERs) and energy storage systems in their premises to locally generate and store energy [1, 2]. With this trend, in near future, the majority of householders are expected to have some types of DERs that are connected to the utility feeder. Thus, merging all the DERs of a group of neighboring householders, it is possible to envision the formation of a small-scale microgrid, referred to as nanogrid [3, 4]. Thus, these neighboring households, denoted in this chapter by community houses, can collectively consume the generated power of the solar photovoltaic-type DERs and battery-type energy storages in grid-connected as well as off-grid statuses.

The majority of the present residential electric appliances work with ac voltage; thus, power electronics-based systems are needed for converting the dc voltage that is generated by photovoltaic-, wind- and battery-type DERs to the ac voltage. Recently, a dc voltage is suggested to supply certain types of residential loads such as lights, TVs, computers directly [5]. A comparison shows that the efficiency of supplying electricity to the residential appliances with a dc voltage of dc generators is greater than the efficiency of supplying them with a converted ac voltage [6, 7]. This improved efficiency is due to the reduction of the power electronics-based conversions. As an example, dc loads such as charging electric vehicles can be supplied directly from the dc bus, eliminating the ac–dc converters. Similarly, the first stage of ac–dc conversion in variable speed drives can be removed with an existing dc bus. This will result in reduced power conversion losses as well as the required power for cooling and ventilation. Additionally, a dc system has reduced copper losses due to lower effective resistance in the conductors, owing to the absence of skin effect and the reactive power flow in the cables [8]. These facts contribute to the increased efficiency of a hybrid ac–dc nanogrid.

Since 2002 that the microgrid concept was introduced [9], numerous researches have been carried out in the area of ac microgrids [10–15]. In recent years, the dc microgrids have also gained the attention of the researchers, thanks to their better efficiency and flexibility in their control. The hierarchical control system and an adaptive droop control of a dc microgrid system are introduced in [16–19], while the control of the DERs in a dc microgrid is studied in [20, 21]. The power electronic interface to connect a dc bus with an ac bus of an MG is introduced in [22], while a current-controlled approach has been utilized in [23] to control the power flow and the power factor of such bidirectional converters.

2 Hybrid AC–DC Nanogrid Structure

With the above review on the existing techniques, this chapter focuses on a limited-size, low-voltage network, denoted by nanogrid, which is assumed as the electric supply system of future small communities. Figure 1 illustrates schematically such a network. The considered nanogrid integrates dc and ac DERs and loads, which are linked to a dc and an ac bus. These two buses are then

interconnected through a power electronics-based converter, referred to as tie-converter. The nanogrid can also exchange power with the utility feeder according to the generation of the DERs. However, it is also capable of operating in off-grid status. The ac bus is also interlinked to the utility feeder via a static switch (SS) and a three-phase power transformer. The ac and dc buses are required to operate individually and independently. However, if there is an increase in power demand or a shortage of power generation which causes voltage deviation in the dc bus or voltage/frequency deviation in the ac bus, the tie-converter takes action to regulate the voltage and frequency.

The AC bus is thought to be a 415-V three-phase system and is assumed to be fed by a 30-kVA transformer, in this chapter. Two DERs are thought to be connected to the ac bus through power electronic converters, while another two power electronic-interfaced DERs are thought to be linked to the dc bus. In this study, it is also supposed that a boosting transformer with a turns ratio of $a = 2$ is used in the structure of the tie-converter. Since uV_{dc} needs to be about 1.35–1.6 of the line voltage of the three-phase system, V_{dc} has been selected as 350 V [24]. If a higher turns ratio is chosen for the transformer, a lower dc voltage can be selected.

The nanogrid should be controlled such that it operates dynamically in the following modes [25]:

Mode-1: isolated and independent ac and dc buses while the ac bus is isolated from the utility feeder,
Mode-2: isolated and independent ac and dc buses while the ac bus is coupled to the utility feeder,
Mode-3: interconnected ac and dc buses while the ac bus is isolated from the utility feeder,
Mode-4: interconnected ac and dc buses while the ac bus is coupled to the utility feeder,

These modes are shown schematically in Fig. 2.

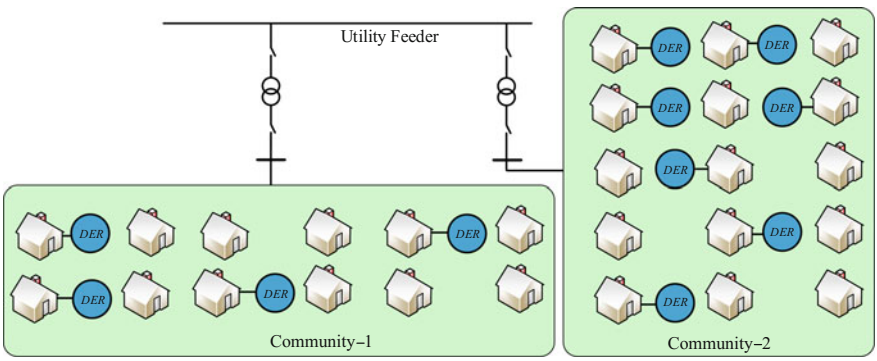

Fig. 1 Schematic illustration of future small community houses

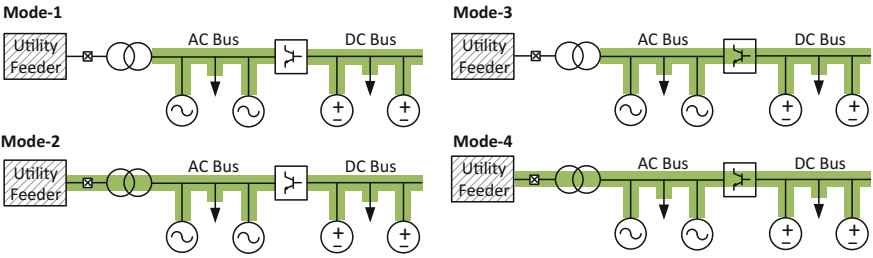

Fig. 2 Different modes of operation of the considered hybrid ac–dc nanogrid

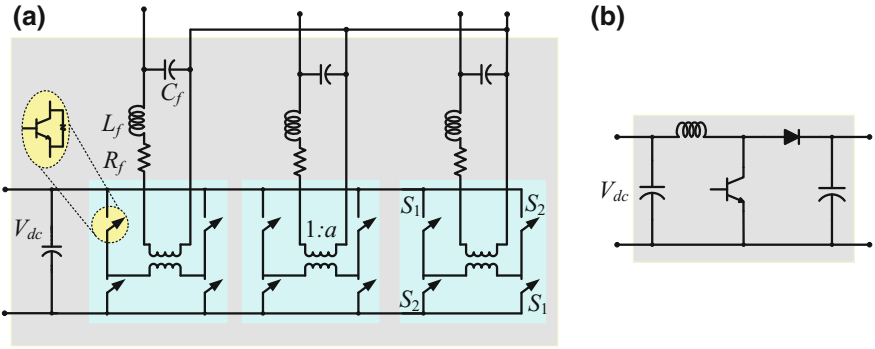

Fig. 3 **a** Considered VSC and filter structure for DERs of ac bus, **b** considered boost converter structure for DERs of dc bus

2.1 AC Bus

A group of DERs and loads form a three-phase ac section. Every DER is coupled to this bus via a three-phase, voltage source converter (VSC) and an LC output filter, as shown schematically in Fig. 3a. Every VSC comprises of three, single-phase H-bridges, while every H-bridge consists of the insulated gate bipolar transistors (IGBTs) and anti-parallel diodes. A single-phase transformer, with 1:a turns ratio, is connected to the output of every H-bridge. The secondary sides of these transformers are star-connected. The transformers offer galvanic isolation for the DERs. This configuration can be utilized to supply single-phase and unbalanced loads since it provides a path for circulation of the zero sequence component of the current. Alternatively, a three-phase, 4-wire (neutral-clamped) VSC can be utilized. However, three-phase, 3-wire VSCs are not suitable as they do not provide a path for the circulation of the zero sequence component of the current and hence cannot be used to supply unbalanced or single-phase loads. It is to be noted that a single-phase ac section can also be formed instead of the three-phase section, when the rating and number of the DERs and loads are small.

In Fig. 3a, the resistance R_f represents the switching and transformer losses, while the inductance L_f and capacitor C_f are connected to the output of the transformers to bypass the switching harmonics. A coupling inductance (L_T) is installed after C_f to provide the desired power sharing ratio among DERs [15].

The control of the ac section of the nanogrid consists of several sections, as discussed below:

2.1.1 Monitoring of SS Status

The nanogrid runs in off-grid or grid-connected status depending on the status of the SS. Isolation of the nanogrid from the utility feeder can be determined by observing the SS status and the availability of a proper data transmission infrastructure to send the data to the DERs. A suitable communication system for microgrids and nanogrids is presented in [26], and its impact on the stability of the system is discussed in [27].

Proper resynchronization should also be carried out before reconnection of the nanogrid to the utility feeder. This can be achieved by monitoring the magnitude and angle of the voltages in both sides of the SS via a phased-locked loop. Thereby, the SS will close only when the voltage magnitude and angles difference in its sides become smaller than a pre-defined minuscule limit. Likewise, a synchronization is also necessary for reconnection of a voltage-controlled DER to the nanogrid.

2.1.2 Control of Output Power

The converters of the DERs in the ac section operate in constant PQ mode, based on maximum power point tracking, when the nanogrid is in grid-connected status. However, they need to operate in voltage-controlled mode, based on droop, in off-grid status. To this end, dissimilar references are necessary for the converter output voltage:

When the nanogrid is in grid-connected status, the utility feeder forces the frequency and voltage in the nanogrid. Thus, the DERs can generate their rated power. Under such conditions, the active (p) and reactive power (q) at the coupling inductance terminal are [15]

$$\begin{aligned} p &= \frac{|V_T| \times |V_{cf}|}{\omega L_T} \sin\left(\delta_{cf} - \delta_T\right) \\ q &= \frac{|V_T|}{\omega L_T} \left(|V_{cf}| \cos\left(\delta_{cf} - \delta_T\right) - |V_T|\right) \end{aligned} \tag{1}$$

where V_T is the voltage of the ac bus side of the coupling inductance, V_{cf} is the voltage across C_f and $V = |V| \angle\delta$ is the phasor representation of $v(t)$. The average active power (P) and reactive power (Q) are derived by passing p and q through a

low-pass filter. Assuming the rated values for the output active and reactive powers and monitoring the voltage of the ac bus, the desired V_{cf} is calculated using (1). This is the voltage reference for the converters in grid-connected status, in Fig. 4.

On the other hand, the frequency and the output voltage of the converters of the DERs are modified according to the droop control and by the help of the pre-defined droop coefficients ($m > 0$, $n > 0$) in off-grid status. In this way, the DERs share the demand in the nanogrid with the specified ratio. The measured output powers of a converter are utilized to define the reference voltage at the converter output as [15]

$$\begin{aligned} \delta_{cf} &= \delta_{\text{ac, rated}} - m\left(P_{\text{ac}} - P_{\text{ac, rated}}\right) \\ \left|V_{cf}\right| &= V_{\text{ac, rated}} - n\left(Q_{\text{ac}} - Q_{\text{ac, rated}}\right) \end{aligned} \tag{2}$$

where the subscript rated shows the rated values and the subscript ac indicates the ac bus.

The block diagram of the control system for the converters of the DERs, connected to the ac bus, is shown in Fig. 4. Note that the SS status monitoring module issues a command to the reference selection block to select the proper reference.

It is to be highlighted that the frequency in the ac bus reduces by $\Delta\omega$ when a DER of this bus increases its output active power from zero to its rated value. Hence, the P–δ droop coefficient for these DERs is

$$m = \frac{\Delta\omega}{P_{\text{rated}}} \tag{3}$$

Assuming $\Delta\omega$ to be constant for all DERs with different ratings, the ratio of P–δ droop coefficient between any two DERs of the ac section of the nanogrid is

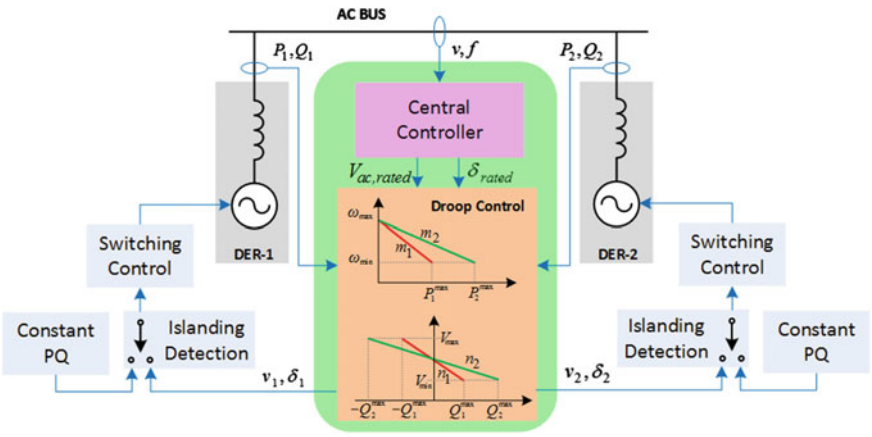

Fig. 4 Control block diagram of the DERs in the ac section of the nanogrid

$$\frac{m_1}{m_2} = \left(\frac{P_{\text{rated},1}}{P_{\text{rated},2}}\right)^{-1} \tag{4}$$

Similarly, the voltage magnitude in the ac bus reduces by ΔV, when a DER increases its output reactive power from zero to its rated value. Thus, the Q–V droop coefficient for these DERs is

$$n = \frac{\Delta V}{Q_{\text{rated}}} \tag{5}$$

Assuming ΔV to be constant for all DERs with different ratings, the ratio of Q–V droop coefficient between any two DERs of the ac section of the nanogrid is

$$\frac{n_1}{n_2} = \left(\frac{Q_{\text{rated},1}}{Q_{\text{rated},2}}\right)^{-1} \tag{6}$$

In [15], it was shown that the output active ratio and reactive power ratio among any two DERs are

$$\frac{P_1}{P_2} \approx \left(\frac{m_1}{m_2}\right)^{-1}, \quad \frac{Q_1}{Q_2} \approx \left(\frac{n_1}{n_2}\right)^{-1} \tag{7}$$

This technique is even suitable when the nanogrid has unbalanced and nonlinear loads, as discussed in [28]. Furthermore, it is also suitable when the nanogrid has an unequal distribution of single-phase DERs in the three-phase system of its ac section, as discussed in [29].

2.1.3 Switching Control of Converter

Converter switching control is in charge of turning on and off the IGBTs of the VSCs appropriately in such a way that the desired voltage is produced across capacitor C_f. This is discussed in detail in [30] and is not repeated here.

2.2 DC Bus

The dc section of the nanogrid is formed by another group of DERs and loads. Every DER is linked to the dc bus via a dc–dc converter. If the dc DER is a battery type, the dc–dc converter needs to be a bidirectional one to facilitate current flow in both directions, while for other DERs, a unidirectional converter is required. Boost converters are used for connecting the DERs to the dc bus in this chapter, as illustrated in Fig. 3b. The size of the inductor and capacitor filters in the dc–dc

converter should be designed to limit the ripples of the current and voltage below acceptable limits. The control of the dc section of the nanogrid consists of several sections, as discussed below:

2.2.1 Monitoring of Tie-Converter Status

The islanding detection of the dc section of the nanogrid is realized by observing the tie-converter status and assuming the availability of a data transmission infrastructure to send these data to the DERs. It is to be noted that connection of the DERs to the dc bus does not need a synchronization technique.

2.2.2 Control of Output Power

The DERs of the dc bus may operate in two modes, based on the status of the tie-converter. When the tie-converter conducts power and the ac and dc buses are connected, the DERs of the dc bus are controlled in constant P mode, based on maximum power point tracking. Thus, the voltage of the dc bus is regulated by controlling the bidirectional power flow over the tie-converter. However, if the tie-converter is off and the buses are disconnected, the dc DERs operate under a droop-based voltage control mode. In such conditions, the output voltage of every DER converter is modified according to the droop control and the designed droop coefficients (m'). In this way, the DERs share the demand of the dc bus with the specified ratio. Hence, the measured output power of a converter (P) is utilized to define the voltage reference for converter output as [16, 17]

$$V_{\mathrm{dc}} = V_{\mathrm{dc,\,rated}} - m'\left(P_{\mathrm{dc}} - P_{\mathrm{dc,\,rated}}\right) \tag{8}$$

where the subscript *dc* denotes the dc bus.

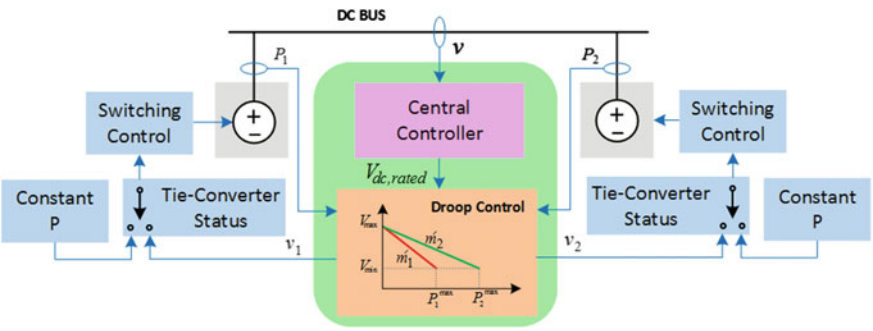

Fig. 5 Control block diagram of the DERs in the dc section of the nanogrid

The control block diagram of the converters of the DERs in the dc section of the nanogrid is shown in Fig. 5. It is to be noted that the tie-converter status monitoring module issues a command to the reference selection block to select the proper reference.

The voltage of the dc bus reduces by ΔV, when a DER of this bus increases its output active power from zero to its rated value. Hence, the P–V droop coefficient for these DERs is

$$m' = \frac{\Delta V}{P_{\text{rated}}} \tag{9}$$

Assuming ΔV to be constant for all DERs with different ratings, the ratio of P–V droop coefficient between any two DERs of the dc section of the nanogrid is

$$\frac{m'_1}{m'_2} = \left(\frac{P_{\text{rated},1}}{P_{\text{rated},2}}\right)^{-1} \tag{10}$$

Thus, it can be shown that the output active power ratio among any two DERs is [15]

$$\frac{P_1}{P_2} \approx \left(\frac{m'_1}{m'_2}\right)^{-1} \tag{11}$$

2.2.3 Switching Control of Converter

Converter switching control is in charge of turning on and off the IGBT in the boost converter (or the dc–dc converters in general) in such a way that the reference voltage is produced across the dc capacitor. This is discussed in detail in [31] and is not repeated here.

2.3 Tie-Converter

The tie-converter has a three-phase VSC, connected to the ac bus, through an LC filter, with a structure similar to those of DERs of the ac section of the nanogrid. In [18, 32], a current-controlled approach is used to control such converters. In this chapter, the voltage-controlled mode of the tie-converter is presented. In this technique, the tie-converter corrects the voltage of its point of common coupling (PCC) in the ac side to a balanced three-phase voltage. To this end, the converter has to exchange reactive power with the ac bus. Moreover, the tie-converter

regulates the voltage of its dc side (i.e., the voltage of the dc bus). This is realized by regulating the voltage angle across C_f of the tie-converter ($\delta_{cf,\ \mathrm{TC},\ \mathrm{ref}}$) from [24]

$$\delta_{cf,\mathrm{TC,ref}} = \left(k_P + \frac{k_I}{s}\right)\left(V_{\mathrm{dc,\ desired}} - \widehat{V}_{\mathrm{dc}}\right) \tag{12}$$

where $\widehat{V}_{\mathrm{dc}}$ is the average of the dc bus voltage, $V_{\mathrm{dc,\ desired}}$ = 350 V in this study, and k_P and k_I are PI coefficients. The tie-converter requires a switching control, similar to the switching control of the DERs of the ac bus.

3 Central Controller of the Nanogrid

The central controller of the nanogrid will regulate the frequency as well as the voltage of the ac bus along with the voltage of the dc bus. This is achieved by regulating the rated values in (2), (8) and (12), as discussed in [33]. This controller gets activated when the ac bus is isolated from the utility feeder. In the case that the frequency or the voltage of the ac bus or the voltage of the dc bus drops below or rise above acceptable pre-defined limits, the central controller takes action to shift down or up the rated values of the droop control. The new rated voltage and rated frequency level are calculated, based on the previous (old) rated levels and the dissimilarity between the actual voltage and frequency and the desired levels, from

$$\begin{aligned} \omega^{\mathrm{new}}_{\mathrm{ac,\ rated}} &= \omega^{\mathrm{old}}_{\mathrm{ac,\ rated}} + 2\pi(f_{\mathrm{desired}} - f) \\ V^{\mathrm{new}}_{\mathrm{ac,\ rated}} &= V^{\mathrm{old}}_{\mathrm{ac,\ rated}} + V_{\mathrm{ac,\ desired}} - |V_{\mathrm{ac}}| \end{aligned} \tag{13}$$

where f and $|V_{\mathrm{ac}}|$ are the frequency and voltage of the ac bus, respectively, while in this chapter, it is thought that $V_{\mathrm{ac,\ desired}}$ = 240 V_{rms} and f_{desired} = 50 Hz. Likewise, the new rated voltage of the dc bus can be calculated from

$$V^{\mathrm{new}}_{\mathrm{dc,\ rated}} = V^{\mathrm{old}}_{\mathrm{dc,\ rated}} + V_{\mathrm{dc,\ desired}} - \widehat{V}_{\mathrm{dc}} \tag{14}$$

It is noteworthy that the central controller has a discrete monitoring time step with a slow time frame.

For the nanogrid system operating in Mode-1 and Mode-3, the central controller acts as the secondary control for every DER of both buses. In such a condition, the central controller defines the rated frequency and voltage for the DERs of the ac section and the rated voltage for the DERs of the dc section, as shown schematically in Fig. 6. In the case that the frequency and the voltage of the ac bus remain below the pre-defined minimum acceptable limits even after the operation of the central controller, load-shedding is required in this bus. When the nanogrid system is operating in Mode-2, the central controller is simply in charge of calculating the rated voltage of the DERs of the dc section. Likewise, if the voltage in the dc bus

remains below the pre-defined minimum acceptable limits even after the operation of the central controller, load-shedding is required in this bus. The central controller is inactive when the nanogrid system operates in Mode-4.

4 Study Cases

The community loads are driven by a specific load profile. Furthermore, the DER generation is variable and intermittent in nature. Thereby, sudden changes in the loads, as well as generations, can be experienced in a nanogrid. Four modes of operation of the nanogrid are evaluated under some study cases here. Let us consider the network shown in Fig. 2 with 2 DERs in the ac bus (i.e., DER-1 and DER-2), 2 DERs in the dc bus (i.e., DER-3 and DER-4), and one load on each bus. The ratio of the nominal capacity of DER-1 and DER-2 is 1:2. Similarly, the ratio of the nominal capacity of DER-3 and DER-4 is 1:2. The studies are conducted based on the technical parameters provided in Table 1.

4.1 Evaluation of Mode-1

Let us assume that neither the tie-converter nor the SS is on. Hence, the ac bus, the dc bus, and the utility feeder are isolated from each other. In such a case, the DERs within both buses share the demand of that bus, and the central controller will control the voltages of the ac and dc bus in the range of ±10% and the frequency of the ac bus in the range of ±0.5 Hz. The nanogrid is thought to be at a steady-state condition initially, with a loading of 5 kW in the ac bus. At t = 1 s, the demand increases by 60% and decreases by 50% at t = 2 s. Figure 7a, b illustrates the output active power and reactive power of DER-1 and DER-2, linked to the ac bus. From this figure, it can be seen that the ratio among DER-1 and DER-2 is maintained as 1:2 during the study. The ac section demand changes are illustrated in Fig. 7c, for the same period. The frequency of the ac bus is illustrated in Fig. 7d and is within ±0.5 Hz boundaries. The voltage rms of the ac bus is shown in

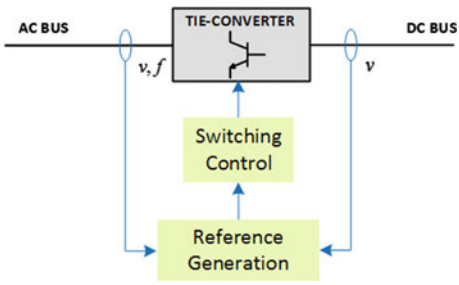

Fig. 6 The control block diagram of the tie-converter of the nanogrid

Table 1 Technical data of the nanogrid network under consideration

Utility feeder	11 kV rms L–L, 50 Hz, R = 0.2 Ω, L = 10 mH
Transformer	30 kVA, 11/0.415 kV, Dyn1, 50 Hz, Z_t = 5%
AC bus	415 Vrms L–L
DC bus	350 V
DERs in AC bus	V_{dc} = 350 V, a = 2, R_f = 0.1 Ω, L_f = 0.36 mH, C_f = 50 μF, L_T = 2.27 mH
	DER-1: $P_{1,\ rated}$ = 2 kW, L_T = 2.27 mH, m_1 = 3.1416 rad/kW, n_1 = 18 V/kVAr DER-2: $P_{2,\ rated}$ = 4 kW, L_T = 1.135 mH, m_2 = 1.5708 rad/kW, n_2 = 9 V/kVAr
DERs in DC bus	DER-3: $P_{3,\ rated}$ = 1 kW, m'_3 = 35 V/kW, V_{dc} = 350 V
	DER-4: $P_{4,\ rated}$ = 2 kW, m'_4 = 17.5 V/kW, V_{dc} = 350 V
Tie-converter (TC)	5 kVA, $V_{dc,\ ref}$ = 350 V, $v_{cf,\ ref}$ = 240 V, a = 2, R_f = 0.1 Ω, L_f = 0.36 mH, C_f = 50 μF

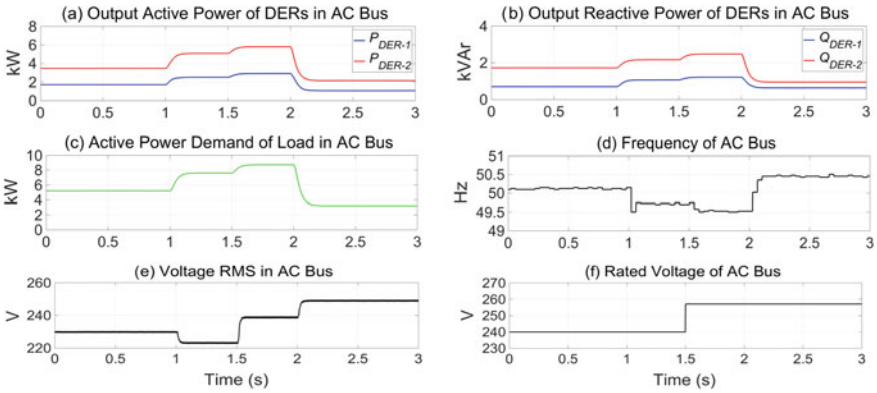

Fig. 7 Analysis outcome for the ac section of the nanogrid bus in Mode-1

Fig. 7e. From this figure, it can be seen that the voltage rms falls below −10% following the demand increase at t = 1 s. Assuming that the central controller has discrete time steps, it applies a modification in the droop curve of the DERs at t = 1.5 s. Hence, the rated voltage of the DERs is increased from 240 to 258 V, as shown in Fig. 7f. As a result of this change, the voltage magnitude of the ac bus restores to 240 V. Following the demand reduction at t = 2 s, the voltage rms of the ac bus increases; however, it is still below +10% limit. Thus, no further action is taken by the central controller.

The DERs of the dc bus supply the demand of this bus. It is assumed that the network is in a steady-state condition initially, with a loading of 3 kW in this bus. This demand increases by 100% at t = 1 s and decreases by 17% at t = 2 s. Figure 8a illustrates the output active power of DER-3 and DER-4, connected to this bus. From this figure, it can be seen that the ratio of the power of these DERs is

sustained as 1:2. Figure 8b illustrates the demand of the dc bus. Figure 8c illustrates the voltage in the dc bus. From this figure, it can be seen that this voltage is retained within ±10% limits; thus, the central controller does not take any actions.

4.2 Evaluation of Mode-2

The tie-converter is thought to be off; thus, the ac bus and the dc bus are disconnected. However, the SS is supposed to be closed; thereby, the ac bus is coupled with the utility feeder. In this condition, the DERs of the ac bus function in constant PQ mode, whereas the DERs of the dc bus run in voltage droop control. The central controller is in charge of controlling the voltage of the dc bus only. Let us assume that the nanogrid is at a steady-state condition initially, with a loading of 7 kW in the ac bus. This demand increases by 29% at $t = 1$ s and decreases at $t = 2$ s by 66%. Figure 9a, b illustrates the output active power and reactive power of DER-1 and DER-2. From this figure, it can be seen that their output powers remain at the rated values at all times. Figure 9c, d illustrates the active and reactive power exchanged between the nanogrid and the utility feeder. From this figure, it can be seen that for $t < 2$ s, the utility feeder supplies a portion of the demand of the ac bus; however, for $t > 2$ s, the ac section of the nanogrid exports power into the utility feeder. The ac bus demand in this period is shown in Fig. 9e. Figure 9f illustrates the frequency of the ac bus. From this figure, it can be seen that the frequency is 50 Hz at all times. Figure 9e illustrates the voltage rms of the ac bus. From this figure, it can be seen that this voltage is not affected.

4.3 Evaluation of Mode-3

Now, let us assume that the tie-converter is on; thereby, the two buses are connected. The SS is thought to be off, and thereby, the nanogrid operates in off-grid

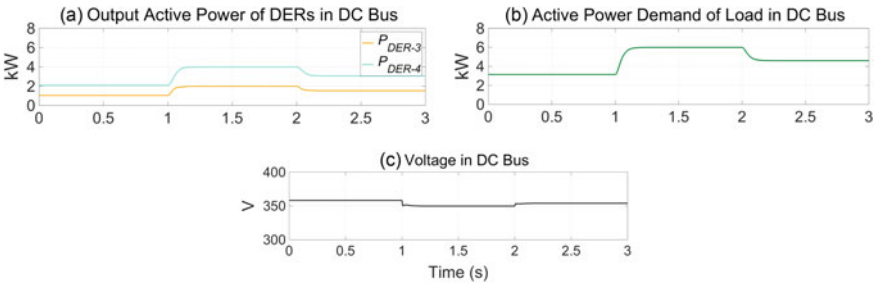

Fig. 8 Analysis outcome for the dc section of the nanogrid bus in Mode-1

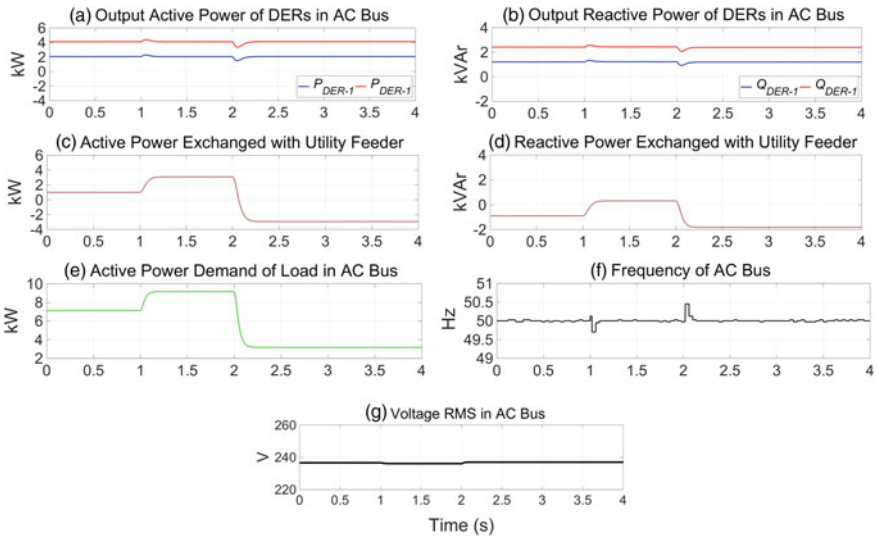

Fig. 9 Analysis outcome for the ac section of the nanogrid bus in Mode-2

mode. Under such a condition, the DERs of each bus supply the demand of that bus, while the tie-converter controls the voltage of both buses. In such a condition, the central controller is the backup of the tie-converter in voltage control. Several scenarios are considered and discussed below:

4.3.1 Demand Change in the AC Section

Let us assume that the nanogrid is at a steady-state condition initially, with a loading of 6 kW in the ac bus. This demand increases by 33% at t = 1 s, although the loading of the dc bus remains constant. Figure 10a illustrates the output active power of DER-1 and DER-2. From this figure, it can be seen that the demand variation is contributed by only these two DERs and the output active power ratio among them is maintained as 1:2. Figure 10b illustrates the output active power of DER-3 and DER-4. From this figure, it can be seen that the DERs of the dc bus do not contribute to this demand variation. The load variation is shown in Fig. 10c. The frequency and the voltage rms of the ac bus are shown, respectively, in Fig. 10d, e. From these figures, it can be seen that both frequency and voltage rms stay within acceptable limits. Figure 10f illustrates the voltage of the dc bus. From this figure, it can be seen that this voltage is not affected.

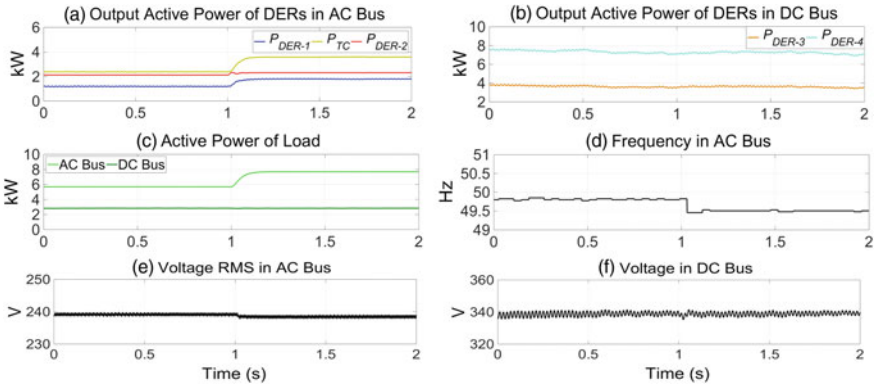

Fig. 10 Analysis outcome for the ac and dc sections of the nanogrid bus in Mode-3 (scenario-A)

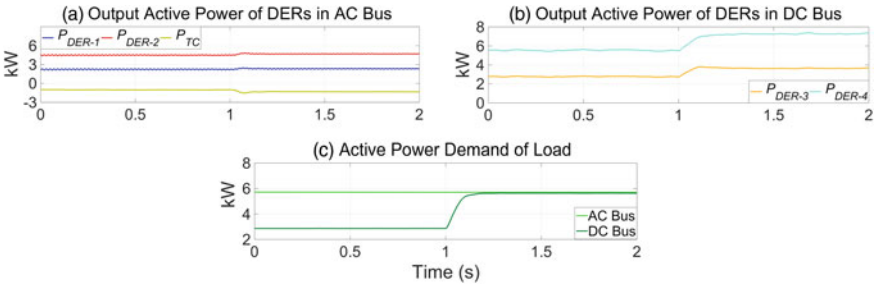

Fig. 11 Analysis outcome for the ac and dc sections of the nanogrid bus in Mode-3 (scenario-B)

4.3.2 Demand Change in the DC Section

Let us consider the nanogrid of scenario-A, with a loading of 3 kW in the dc bus. This demand increases by 100% at $t = 1$ s. Figure 11a illustrates the output active power of DER-1 and DER-2. From this figure, it can be seen that the output powers of the DERs of the ac bus are not affected by this demand variation. Thereby, the voltage rms and frequency of this bus will not be affected, either. Figure 11b illustrates the output active powers of DER-3 and DER-4. From this figure, it can be seen that these two DERs contribute to the demand variation, while the ratio of their output powers is maintained as 1:2. The demand variation is shown in Fig. 11c.

4.3.3 AC Bus DERs Operating in Maximum Capacity

Let us consider the nanogrid of scenario-A, where the DERs of the ac bus are thought to be operating in their maximum ratings. In this condition, the demand of the ac bus is approximately 6 kW where its 33% is supplied by the dc bus, through

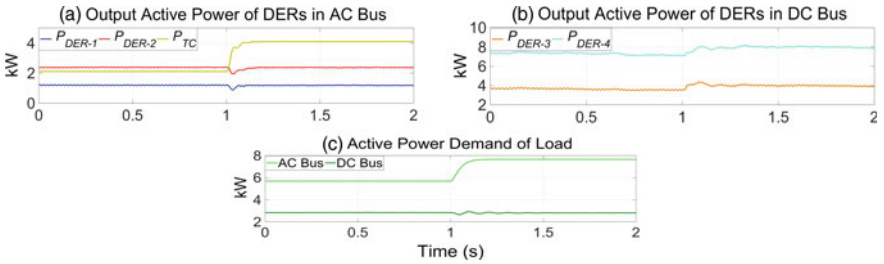

Fig. 12 Analysis outcome for the ac and dc sections of the nanogrid bus in Mode-3 (scenario-C)

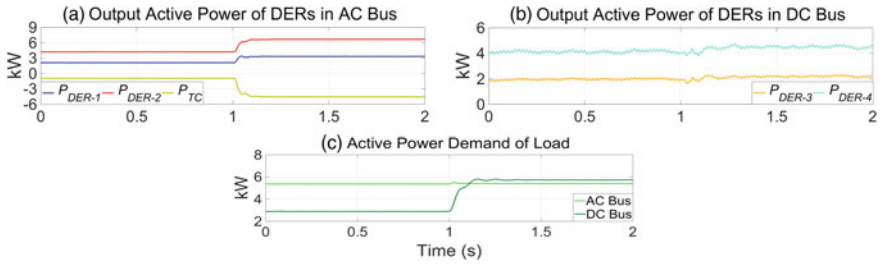

Fig. 13 Analysis outcome for the ac and dc sections of the nanogrid bus in Mode-3 (scenario-D)

the tie-converter. At $t = 1$ s, the demand of the ac bus increases by 30%. Figure 12a illustrates the output active power of the DER-1 and DER-2. From this figure, it can be seen that the output power of these DERs remains unaffected at their maximum capacities. Hence, the DERs in the dc bus contribute to this extra load and the power transfer over the tie-converter increases. Figure 12b illustrates the output active power of DER-3 and DER-4. From this figure, it can be seen that the output power of the DERs of the dc bus increases but is maintained as 1:2. The demand variations in the ac bus of the nanogrid are illustrated in Fig. 12c.

4.3.4 DC Bus DERs Operating in Maximum Ratings

Let us consider the nanogrid of scenario-B, where the DERs of the dc bus are operating in their maximum capacities. In this condition, the demand of the dc bus is 3 kW, while the DERs connected to this bus generate 6 kW. Therefore, the rest of the generated power is exported to the ac section through the tie-converter. Figure 13a illustrates the output active power of DER-1 and DER-2, as well as the active power, injected to the ac bus through the tie-converter. From this figure, it can be seen that only 1 kW is delivered to the ac bus through the tie-converter due to its power losses. At $t = 1$ s, the demand of the dc bus increases by 100%. Hence, the DERs of the ac bus contribute to this extra demand and the power transfer over the TC increases by 3 kW. As shown in Fig. 13a, the ratio of the output active

power among the DER-1 and DER-2 is maintained as 1:2. Figure 13b illustrates the output active power of the DER-3 and DER-4. From this figure, it can be seen that the output power of these DERs remained as before. The demand variations in the nanogrid are illustrated in Fig. 13c.

4.4 Evaluation of Mode-4

Now, let us assume that both of the tie-converter and the SS are on; thereby, the buses are connected, and the nanogrid is operating in grid-connected mode. Under such a condition, the DERs of the ac bus function in constant PQ mode. Likewise, the DERs of the dc bus function in constant P mode. The extra demand of the nanogrid is supplied by the utility feeder, or the surplus power produced by the DERs is exported to the utility feeder. Let us assume that the nanogrid network is at a steady-state condition initially, with a loading of 4 kW in the ac bus and 1 kW in the dc bus. A load increase of 150% occurs in the ac bus at $t = 1$ s, while a load increase of 500% occurs in the dc bus at $t = 2$ s. Figure 14a, b illustrates the output active power of all the DERs, in both buses. From these figures, it can be seen that the ratio of the output powers is maintained as desired. For $t < 1$ s, the excess generated power by the DERs of the dc bus, minus the tie-converter losses, is delivered to the ac bus. Likewise, the excess power of the ac bus is exported to the utility feeder, as shown in Fig. 11c. As the demand of the ac bus increases at $t = 1$ s, the power transferred through the tie-converter remains unaffected. In such a condition, as the levels of the generated and consumed power in the ac bus are the same, the level of the exchanged power between the nanogrid and the utility feeder becomes zero. As the demand of the dc bus increases at $t = 2$ s, the direction of the transferred power via the tie-converter is inverted, and it takes 2 kW from the ac bus.

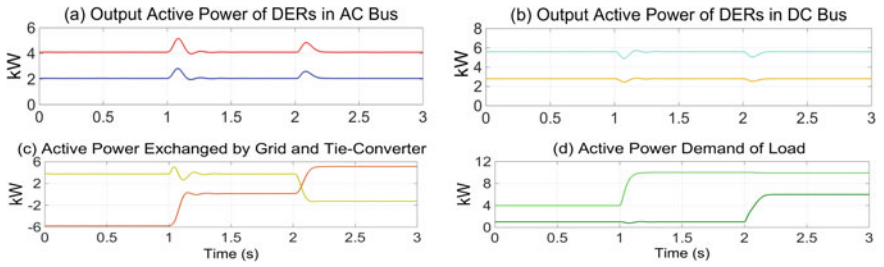

Fig. 14 Analysis outcome for the ac and dc sections of the nanogrid bus in Mode-4

5 Conclusion

This chapter presented the structure of a small-scale nanogrid system which facilitates the integration of renewable energy-based DERs in the electrical system of future community houses. This is an important technique for increasing the penetration of renewable energies for electricity generation and increases the sustainability of the electricity generation area. The nanogrid structure accommodates the ac and dc connection of the resources and supplies both dc- and ac-type loads within the community households. The two buses are interconnected via a tie-converter, which is in charge of controlling the voltage in both of them as it can facilitate a bidirectional power transfer between the buses. The chapter presented the primary control of each source as well as the central controller of the nanogrid. Four different operation modes are possible, based on the connection/disconnection status of the ac and the dc bus and the connection/disconnection status of the nanogrid with the utility feeder, as discussed in detail in the chapter.

References

1. L.A. de Souza Ribeiro, O.R. Saavedra, S.L. de Lima, and J. Gomes de Matos, "Isolated micro-grids with renewable hybrid generation: The case of Lençóis island," *IEEE Trans. on Sustainable Energy*, Vol. 2, No. 1, pp. 1–11, Jan. 2011.
2. M.V. Kirthiga, S.A. Daniel and S. Gurunathan, "A methodology for transforming an existing distribution network into a sustainable autonomous micro-Grid," *IEEE Trans. on Sustainable Energy*, Vol. 4, No. 1, pp. 31–41, Jan. 2013.
3. J. Bryan, R. Duke and S. Round, "Decentralized generator scheduling in a nanogrid using DC bus signaling," IEEE Power Engineering Society General Meeting, pp. 977–982, Vol. 1, June 2004.
4. R. P. S. Chandrasena, F. Shahnia, A. Ghosh and S. Rajakaruna, "Operation and control of a hybrid AC-DC nanogrid for future community houses," 24th Australasian Universities Power Engineering Conference (AUPEC), pp. 1–6, Australia, 2014.
5. A. Sannino, G. Postiglione and M.H.J. Bollen, "Feasibility of a DC network for commercial facilities," *IEEE Trans. on Industry Applications*, Vol. 39, No. 5, pp. 1499–1507, Sept./Oct. 2003.
6. N. Eghtedarpour and E. Farjah, "Distributed charge/discharge control of energy storages in a renewable-energy-based DC micro-grid," *IET Renewable Power Generation*, Vol. 8, No. 1, pp. 45–57, Jan. 2014.
7. N. Eghtedarpour and E. Farjah, "Power Control and Management in a Hybrid AC/DC Microgrid," *IEEE Transaction on Smart Grid*, Vol. 5, No. 3, pp. 1494–1505, May 2014.
8. C. Liang and M. Shahidehpour, "DC Microgrids: Economic Operation and Enhancement of Resilience by Hierarchical Control", *IEEE Transaction on Smart Grid*, Vol. 5, No. 5, pp. 2517–2526, Sept. 2014.
9. R.H. Lasseter, "Microgrids: distributed power generation," IEEE Power Engineering Society Winter Meeting, Vol. 1, pp. 146–149, 2001.
10. K. Jaehong, J.M. Guerrero, P. Rodriguez, et al. "Mode adaptive droop control with virtual output impedances for an inverter-based flexible ac microgrid," *IEEE Trans. on Power Electronics*, Vol. 26, No. 3, pp. 689–701, March 2011.

11. M. Savaghebi, A. Jalilian, J.C. Vasquez and J.M. Guerrero, "Secondary control scheme for voltage unbalance compensation in an islanded droop-controlled microgrid," *IEEE Trans. on Smart Grid*, Vol. 3, No. 2, pp. 797–807, June 2012.
12. F. Katiraei and M.R. Iravani, "Power management strategies for a microgrid with multiple distributed generation units," *IEEE Trans. on Power Systems*, Vol. 21, No. 4, pp. 1821–1831, Nov. 2006.
13. A. Mehrizi-Sani and R. Iravani, "Online set point modulation to enhance microgrid dynamic response: Theoretical foundation," *IEEE Trans. on Power Systems*, Vol. 27, No. 4, pp. 2167–2174, Nov. 2012.
14. M.B. Delghavi and A. Yazdani, "Islanded-mode control of electronically coupled distributed-resource units under unbalanced and nonlinear load conditions," *IEEE Trans. on Power Delivery*, Vol. 26, No. 2, pp. 661–673, April 2011.
15. F. Shahnia, R.P.S. Chandrasena, S. Rajakaruna and A. Ghosh, "Primary control level of parallel DER converters in system of multiple interconnected autonomous microgrids within self-healing networks," *IET Generation Trans. & Distribution*, Vol. 8, Issue 2, pp. 203–222, 2014.
16. X. Lu; J.M. Guerrero, S. Kai and J.C. Vasquez, "An improved droop control method for dc microgrids based on low bandwidth communication with dc bus voltage restoration and enhanced current sharing accuracy," *IEEE Trans. on Power Electronics*, Vol. 29, No. 4, pp. 1800–1812, April 2014.
17. T. Dragicevic, J.M. Guerrero, J.C. Vasquez and D. Skrlec, "Supervisory control of an adaptive-droop regulated dc microgrid with battery management capability," *IEEE Trans. on Power Electronics*, Vol. 29, No. 2, pp. 695–706, Feb. 2014.
18. P. C. Loh, Ding Li, Yi Kang Chai, and F. Blaabjerg, "Autonomous Operation of Hybrid Microgrid with AC and DC Subgrids," *IEEE Trans. on Power Electronics*, Vol. 28, No. 5, pp. 2214–2223, May 2013.
19. Xiaonan Lu, J. M. Guerrero, Kai Sun, J. C. Vasquez, R. Teodorescu, and Lipei Huang, "Hierarchical Control of Parallel AC-DC Converter Interfaces for Hybrid Microgrids," *IEEE Trans. on Smart Grid*, Vol. 5, No. 2, pp. 683–692, Mar. 2014.
20. Y. Ito, Y. Zhongqing and H. Akagi, "DC microgrid based distribution power generation system," IEEE 4th Int. Power Electronics and Motion Control Conf. (IPEMC), Vol. 3, pp. 1740–1745, Aug. 2004.
21. L. Xu and D. Chen, "Control and operation of a DC microgrid with variable generation and energy storage," *IEEE Trans. on Power Delivery*, Vol. 26, No. 4, pp. 2513–2522, Oct. 2011.
22. Z. Jiang and X. Yu, "Power electronics interfaces for hybrid DC and AC-linked microgrids," IEEE 6th Int. Power Electronics and Motion Control Conf. (IPEMC) pp. 730–736, May 2009.
23. P. Shanthi, U. Govindarajan, and D. Parvathyshankar, "Instantaneous power-based current control scheme for VAR compensation in hybrid AC/DC networks for smart grid applications," *IET Power Electronic.*, Vol. 7, No. 5, pp. 1216–1226, May 2014.
24. A. Ghosh and G. Ledwich, *Power Quality Enhancement using Custom Power Devices*, Kluwer Academic, 2002.
25. R. P. S. Chandrasena, F. Shahnia, S. Rajakaruna and A. Ghosh, "Dynamic operation and control of a hybrid nanogrid system for future community houses," *IET Generation, Transmission & Distribution*, vol. 9, no. 11, pp. 1168–1178, 2015.
26. M.A. Setiawan, F. Shahnia, R.P.S. Chandrasena and A. Ghosh, "Data communication network and its delay effect on the dynamic operation of distributed generation units in a microgrid," Power and Energy Engineering Conference (APPEEC), 2014 IEEE PES Asia-Pacific, Hong Kong, 2014, pp. 1–6.
27. M.A. Setiawan, F. Shahnia, S. Rajakaruna and A. Ghosh, "ZigBee-based communication system for data transfer within future microgrids," *IEEE Trans. on Smart Grid*, vol. 6, no. 5, pp. 2343–2355, 2015.
28. R.P.S. Chandrasena, F. Shahnia, S. Rajakaruna and A. Ghosh, "Control, operation and power sharing among parallel converter-interfaced DERs in a microgrid in the presence of

unbalanced and harmonic loads," 23rd Australasian Universities Power Engineering Conference (AUPEC), pp. 1–6, Australia, 2013.
29. F. Shahnia, and R.P.S. Chandrasena, "A three-phase community microgrid comprised of single-phase energy resources with an uneven scattering amongst phases," *International Journal of Electrical Power & Energy Systems*, Vol. 84, pp. 267–283, 2017.
30. F. Shahnia, S.M. Ami, and A. Ghosh, "Circulating the reverse flowing surplus power generated by single-phase DERs among the three phases of the distribution lines," *International Journal of Electrical Power & Energy Systems*, Vol. 76, pp. 90–106, March 2016.
31. N. Mohan, T.M. Undeland, and W.P. Robbins, *Power Electronics: Converters, Applications, and Design*, Wiley, 2002.
32. X. Liu, P. Wang and P.C. Loh, "A hybrid AC/DC microgrid and its coordination control," *IEEE Trans. on Smart Grid*, Vol. 2, No. 2, pp. 278–286, June 2011.
33. R.P.S. Chandrasena, F. Shahnia, A. Ghosh and S. Rajakaruna, "Secondary control in microgrids for dynamic power sharing and voltage/frequency adjustment," 24th Australasian Universities Power Engineering Conference (AUPEC), pp. 1–8, Australia, 2014.

http://www.springer.com/978-3-319-54806-7

Sustainable Development in Energy Systems
Azzopardi, B. (Ed.)
2017, XIV, 231 p. 115 illus., Hardcover
ISBN: 978-3-319-54806-7